



Research article

Performance of magnetic dipole contribution on ferromagnetic non-Newtonian radiative MHD blood flow: An application of biotechnology and medical sciences

G. Dharmiah^a, J.L. Rama Prasad^b, K.S. Balamurugan^c, I. Nurhidayat^d, Unai Fernandez-Gamiz^e, S. Noeiaghdam^{f,g,*}

^a Department of Mathematics, Narasaraopeta Engineering College, Narasaraopet, A.P., India

^b Department of Mathematics, PB Siddartha College of Arts and Science, Vijayawada, A.P., India

^c Department of Mathematics, RVR & JC College of Engineering, Guntur, A.P., India

^d Department of Mathematics, School of Science, King Mongkut's Institute of Technology Ladkrabang, Bangkok, 10520, Thailand

^e Nuclear Engineering and Fluid Mechanics Department, University of the Basque Country UPV/EHU, Nieves Cano 12, 01006, Vitoria-Gasteiz, Spain

^f Industrial Mathematics Laboratory, Baikal School of BRICS, Irkutsk National Research Technical University, Irkutsk, 664074, Russia

^g Department of Applied Mathematics and Programming, South Ural State University, Lenin Prospect 76, Chelyabinsk, 454080, Russia



ARTICLE INFO

Keywords:

Slip conditions
Magnetohydrodynamic
Casson fluid
Stretching sheet
Radiation
Magnetic dipole

ABSTRACT

Casson flow ferromagnetic liquid blood flow over stretching region is studied numerically. The domain is influence by radiation and blood flow velocity and thermal slip conditions. Blood acts an impenetrable magneto-dynamic liquid yields governing equations. The conservative governing nonlinear partial differential equations, reduced to ODEs by the help of similarity translation technique. The transport equations were transformed into first order ODEs and the resultant system are solved with help of 4th order R-K scheme. Performing a magnetic dipole with a Casson flow across a stretched region with Brownian motion and Thermophoresis is novelty of the problem. Significant applications of the study in some spheres are metallurgy, extrusion of polymers, production in papers and rubber manufactured sheets. Electronics, analytical instruments, medicine, friction reduction, angular momentum shift, heat transmission, etc. are only few of the many uses for ferromagnetic fluids. As ferromagnetic interaction parameter value improves, the skin-friction, Sherwood and Nusselt numbers depreciates. A comparative study of the present numerical scheme for specific situations reveals a splendid correlation with earlier published work. A change in blood flow velocity magnitude has been noted due to Casson parameter. Increasing change in blood flow temperature noted due to Casson parameter. Skin-friction strengthened and Nusselt number is declined with Casson parameter. The limitation of current work is a non-invasive magnetic blood flow collection system using commercially available magnetic sensors instead of SQUID or electrodes.

* Corresponding author. Industrial Mathematics Laboratory, Baikal School of BRICS, Irkutsk National Research Technical University, Irkutsk, 664074, Russia.

E-mail addresses: dharmia.g2007@gmail.com (G. Dharmiah), jlrprasad@gmail.com (J.L.R. Prasad), muruganbalaks@gmail.com (K.S. Balamurugan), irfannurhidayat09@gmail.com (I. Nurhidayat), unai.fernandez@ehu.eus (U. Fernandez-Gamiz), snoei@istu.edu, noiagdams@susu.ru (S. Noeiaghdam).

<https://doi.org/10.1016/j.heliyon.2023.e13369>

Received 14 August 2022; Received in revised form 15 January 2023; Accepted 28 January 2023

Available online 1 February 2023

2405-8440/© 2023 The Authors. Published by Elsevier Ltd. This is an open access article under the CC BY-NC-ND license (<http://creativecommons.org/licenses/by-nc-nd/4.0/>).

1. Introduction

Fluid dynamical behaviour of biological liquids in the presence of a magnetic impact is an emerging field of study in expanding field. In the case of hypertension and associated disorders, a magnetic field has been shown to be effective in lowering blood pressure. Potential medical applications make BFD (biomagnetic fluid dynamics) analysis increasingly appealing. Hyperthermia, medication delivery through magnetic particles for the treatment of malignant tumours, and cell separation for magnetic devices are only a few of the medical uses presented. The circulatory system of the human body consists of capillaries, arteries, and veins via which blood travels throughout the body. Blood travels via the capillaries in the skin and the muscles, the arteries leave the heart, and the veins return the blood. Murtaza et al. [1] scrutinized two-dimensional time-dependent blood flow across a stretched region with a high magnetic field. Effects of an external magnetic field gradient on a steady, incompressible, viscous biomagnetic liquid were scrutinized by Murtaza et al. [2]. Using the Navier-Stokes equation, [3] analyzed higher wall shear stress was seen for medium porosity during pulsatile blood flow. Model for blood pulsatile flow owing to periodic body acceleration was established in Ref. [4]. Pathological blood vessel modeling and numerical solution using finite difference [5]. Alam et al. [6] scrutinized the biomagnetic flow and blood heat transmission contains nano-gold particles across a stretched region with a magnetic dipole. This issue used MHD and FHD concepts. Olubode et al. [7] studied an effect of Gold Carreau nanofluid slip and buoyancy and found to be high values enhance velocity. Many researchers explored their research in the presence of stretched sheet along with non-Newtonian fluids [8–16].

Fluid flow and heat transfer mechanism have ample applications in science and engineering field. Convective non-Newtonian fluid attracts researchers to examine their thermo-physical properties. The movement of Casson fluids is crucial in many areas of contemporary engineering and industry. Shampoo, tooth paste, glass fiber, plastic film design, blood therapy, and custard solution are just a few examples of products that find use in industry. Non-Newtonian fluids are used many engineering applications and food processing industries, including the production of condensed milk, sugar solutions, and tomato sauce. Casson fluid's blood flow velocity, heat, and transportation may be modulated using a varying magnetic field to meet the needs of industrial engineering and food production management. Recent fuel cell technologies and materials manufacturing both place a premium on the study of heat transport in enclosed spaces (cavities) (crystal growth etc). As a result, engineers have reported convection flows in enclosures filled with non-Newtonian fluid extensively, both experimentally and via a number of modeling methodologies. Various scholars have examined both isotropic and anisotropic media.

Akinbobola et al. [17] studied variable conductivity influence on non-Newtonian second grade flow via stretched region with blood flow temperature. Rasool et al. [18] discussed Casson nanofluid embedded porous medium through Darcy-Forchheimer model. Abdelmalek et al. [19] addressed Arrhenius activation energy and Stefan blowing impact on mass transfer characteristics. Soret effect and Chemically reaction impacts on Casson liquid on a vertical region executed by Charan et al. [20]. Chemical reaction impact on Casson liquid across a vertical surface done by Vedavati et al. [21].

Ferrofluids are tiny ferromagnetic acarids suspended in a fluid carriers and magnetized under the regulation of a magnetic region [22] and has several applications. Ferrofluids are utilized in a variety of appurtenances, including lasers, avionics, nuclear plants, X-rays, crystal processing, fiber optics, robotics, textile tools, refrigeration, loudspeakers, and peripherals of computers [23]. The liquid flow over a stretched membrane has become a classic fluid dynamical issue due to the fact that it possesses an easy closed structure solution. Several researchers, motivated by industrial manufacturing applications, analyzed the varied liquid flows across stretched sheets. Rasool et al. [24] investigated mass and heat transport for a nonlinearly stretched membrane using the Darcy–Forchheimer connection. Recent efforts in the fields of heat transfer and stretched regions can be found in Refs. [25,26].

Research into the effects of radiation on blood flow is vital, since it has substantial implications for biomedical engineering and many types of medical therapy, most notably thermal therapeutic techniques. One common method for applying heat to different areas of the human body is by use of infrared radiation. As infrared radiation may be used to warm the blood capillaries in the afflicted regions without first having to warm the surrounding tissue, this method is favoured in heat treatment. Heat therapy has been shown to be useful in the treatment of muscular spasms and persistent widespread pain. Researchers have conducted a number of experiments to evaluate infrared/ultrasonic radiation's blood flow impacts (cf. Kobu [27], Inoue and Kabaya [28], and Nishimoto et al. [29]).

Arterial tree is responsible for transporting a lot of heat to various regions of the body as blood flows through it. Heat may be transferred over the skin's surface in four ways: radiation and evaporation. Radiative heat transfer is often understood to include the transmission of energy by electromagnetic waves across empty space. An amount of heat that blood can transport depends on various factors, including the (i) blood's heat transfer coefficient, (ii) blood density, (iii) blood flow blood flow velocity, and (iv) the artery's radius. Heat transferred blood amount may be thought to rely simply on heat transferred blood and the arterial radius and other factors. It's also worth noting that a man's blood flow increases when he engages in strenuous physical labor and when his body is subjected to extreme heat. The blood flow cannot be maintained normally under these conditions. The artery's size must increase according to the rise in blood flow. It is well-known that when the ambient blood flow temperature is more than 200° Celsius, heat is lost from the skin by evaporation via sweating, and that when the ambient blood flow temperature is lower than 200° Celsius, heat is lost from the human body via conduction and radiation. Ogulu and Bestman [30] based their discussion of blood flow with radiative heat transfer on a theoretical investigation. In terms of blood's magnetic response, the iron in hemoglobin molecules is responsible for the paramagnetic component, while the hydrogen, carbon atoms, nitrogen, and oxygen, in vessel tissues are responsible for the diamagnetic component. Being that the erythrocyte is a primary biomagnetic material, it is probable that with an external magnetic field would affect flow of blood. Chen [31] hypothetically considered magnetic influence on blood flow. Biomagnetic flow across a stretched surface proposed by Tzirtzilakis and Tanoudis [32].

The purpose of this model is to investigate how a sheet stretch affects the blood flow of a Casson ferromagnetic fluid. The literature review reveals that, in the presence of diverse external forces, researchers have looked at flow liquids and heat transfer liquids across a

stretched region. As per author’s best knowledge, no prior research has examined the effect of blood flow velocity and blood flow temperature slips through the casson blood flow ferromagnetic liquid across a stretched sheet over a broad range of fluid-controlling governing parameters to investigate heat transfer characteristics. Several theoretical estimations of parameters that control the physical issue are provided.

2. Mathematical model and governing equations

The diagram of the current physical action is illustrated in Fig. 1. A domain of interest is blood passes via stretching region with $U_w(x, t) = \frac{ax}{1-ct}$.

The assumptions of the problem are:

- > X-axis takes place on the surface.
- > Y-axis takes place normal to that.
- > Constants a and c \ni , $a > 0, c \geq 0$ and $ct < 1$.
- > The blood flow temperature T_w is constant and T_∞ is ambient fluid blood flow temperature with $T_w < T_\infty$.
- > The magnetic potency $B(t) = \frac{B_0}{(1-ct)^{\frac{1}{2}}}$ is implemented in y-direction.
- > At $t = 0$, the magnetic field is constant.
- > The magnetic strength for a magnetic dipole is ‘H’ and is located with distance ‘d’.
- > Human body blood flow temperature $T_w = 37^\circ\text{C}$
- > The body curie blood flow temperature $T_\infty = 41^\circ\text{C}$
- > For blood fluid assuming values $\mu = \frac{3.2}{10^3}$ kg/ms; $\rho = 1050$ [kg/m³]; $\kappa = 2.2 \times 10^{-3}$ [J/msK]; $C_p = 14.65$ [J/kg.K]; $Pr = 21$ (Ref.[33]).

The tensor equations are given by

$$\tau^{\frac{1}{2}} = \tau_0^{\frac{1}{2}} + \mu\gamma^{\frac{1}{2}}$$

$$\tau_{ij} = \begin{cases} 2 e_{ij} \left(\mu_B + \frac{P_y}{\sqrt{2\pi}} \right), \pi > \pi_c \\ 2e_{ij} \left(\mu_B + \frac{P_y}{\sqrt{2\pi_c}} \right), \pi_c > \pi \end{cases} \tag{1}$$

The above assumptions lead to following governing equations [34]:

$$\frac{\partial u}{\partial x} + \frac{\partial u}{\partial y} = 0 \tag{2}$$

$$\frac{\partial u}{\partial t} + u \frac{\partial u}{\partial x} + v \frac{\partial u}{\partial y} = v \left(1 + \frac{1}{B} \right) \frac{\partial^2 u}{\partial y^2} - \frac{v}{k_1(t)} u + \frac{\mu_0 M_1}{\rho} \frac{\partial H}{\partial x} - \frac{\sigma}{\rho} B^2(t) u \tag{3}$$

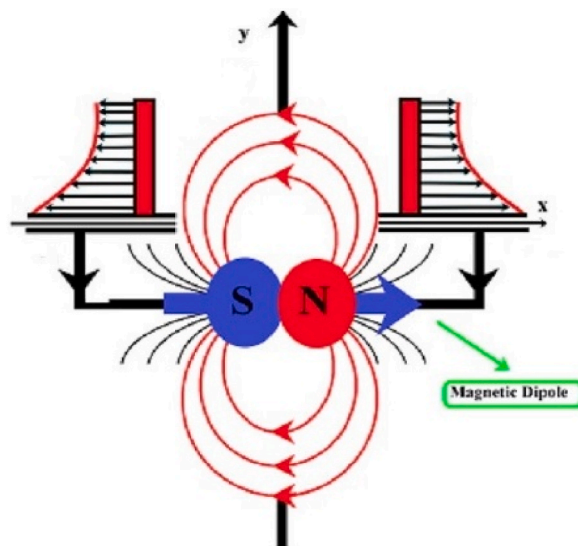


Fig. 1. Physical flow diagram.

$$\frac{\partial T}{\partial t} + u \frac{\partial T}{\partial x} + v \frac{\partial T}{\partial y} = \frac{\kappa}{\rho C_p} \frac{\partial^2 T}{\partial y^2} - \frac{1}{\rho C_p} \frac{\partial q_r}{\partial y} - \frac{\mu_0 T}{\rho C_p} \frac{\partial M_1}{\partial T} \left(u \frac{\partial H}{\partial x} + v \frac{\partial H}{\partial y} \right) \tag{4}$$

$$\frac{\partial C}{\partial t} + u \frac{\partial C}{\partial x} + v \frac{\partial C}{\partial y} = D_B \frac{\partial^2 C}{\partial y^2} + \frac{D_T}{T_\infty} \frac{\partial^2 T}{\partial y^2} \tag{5}$$

The corresponding boundaries are [35]:

$$u = U_w + N\mu \frac{\partial u}{\partial y}, v = V_w, T = T_w + \frac{\partial T}{\partial y}, \frac{\partial T}{\partial y} \frac{D_T}{T_\infty} + \frac{\partial C}{\partial y} D_B = 0 \text{ at } y = 0 \tag{6}$$

$$u \rightarrow 0, T \rightarrow T_\infty, C \rightarrow C_\infty \text{ as } y \rightarrow \infty \tag{7}$$

The heat flux q_r and T^4 are considered from [36–38]

$$q_r = \frac{4}{3} \frac{\sigma^*}{k^*} \frac{\partial T^4}{\partial y} \tag{8}$$

and

$$T^4 \cong 4TT_\infty^3 - 3T_\infty^4 \tag{9}$$

In RHS of third term in Eq. (3) is called as the ferromagnetic body force per unit volume. In RHS of third term in Eq. (4) is called heating due to adiabatic magnetization.

The scalar magnetic potential, its components and magnitude of magnetic field \mathbf{H} are [39].

$$\Phi = \frac{\gamma}{2\pi} \frac{x}{x^2 + (y+a)^2} \tag{10}$$

$$H_x = -\frac{\partial V}{\partial x} = \frac{\gamma}{2\pi} \frac{x^2 - (y+d)^2}{[x^2 + (y+d)^2]^2} \tag{11}$$

$$H_y = -\frac{\partial V}{\partial y} = \frac{\gamma}{2\pi} \frac{2x(y+d)}{[x^2 + (y+d)^2]^2} \tag{12}$$

$$\|H\| = \left\{ \left(\frac{\partial H}{\partial x} \right)^2 + \left(\frac{\partial H}{\partial y} \right)^2 \right\}^{\frac{1}{2}} \tag{13}$$

Eqs. (11) and (12) gives

$$\frac{\partial H}{\partial x} = -\frac{\gamma}{2\pi} \frac{2x}{(y+d)^4} \tag{14}$$

$$\frac{\partial H}{\partial y} = \frac{\gamma}{2\pi} \left\{ \frac{-2}{(y+d)^3} + \frac{4x^2}{(y+d)^5} \right\} \tag{15}$$

Introducing similarity variables

$$\begin{aligned} k_1(t) &= k_2(1-ct); V_w = -\sqrt{\frac{vU_w}{x}} f(0); N = N_0(1-ct)^{\frac{1}{2}}; K = K_0(1-ct)^{\frac{1}{2}}; V = \frac{\alpha}{2\pi} \frac{x}{x^2 + (y+d)^2}; \\ \alpha &= \sqrt{\frac{U_w}{vx}} d; M_1 = K(T - T_\infty); \eta = \sqrt{\frac{U_w}{vx}} y; \psi = \sqrt{vxU_w} f(\eta); \theta(\eta) = \frac{T - T_\infty}{T_w - T_\infty}; s_t = K_0 \sqrt{\frac{a}{v}}; s_f = N_0 \rho \sqrt{av}; \\ \alpha &= \sqrt{\frac{U_w}{x}} d; \varepsilon = \frac{T_\infty}{T_w - T_\infty}; M = B_0 \sqrt{\frac{\sigma}{\rho a}}; A = \frac{c}{a}; k_3 = \frac{ak_2}{v}; Nr = \frac{16\sigma^* T_\infty^3}{3kk^*}; \beta = \frac{\gamma}{2\pi} \frac{\mu_0 K \rho (T_w - T_\infty)}{\mu^2}; \\ \lambda &= \frac{a\mu^2}{\rho k (T_w - T_\infty) (1-ct)}; Le = \frac{v}{D_B}; Nt = \frac{D_T (\rho C)_p (T_w - T_\infty)}{T_\infty \nu (\rho C)_f}; Nb = \frac{D_B (\rho C)_p (C_w - C_\infty)}{\nu (\rho C)_f} \end{aligned} \tag{16}$$

Using similarity transformations, above equations transformed into the following manner.

$$\left(1 + \frac{1}{B} \right) f''' + ff'' - f'^2 - M^2 f' - \frac{f'}{k_3} - \frac{2\beta\theta}{(\eta + \alpha)^4} - A \left(f' + \frac{\eta f''}{2} \right) = 0 \tag{17}$$

$$\frac{(1 + Nr)}{\text{Pr}}\theta'' - f'\theta + f\theta' - \frac{2\beta\lambda(\varepsilon + \theta)}{\text{Pr}(\eta + \alpha)^3}f - A\left[\theta + \frac{\eta\theta'}{2}\right] = 0 \tag{18}$$

$$\varphi'' + \text{Le}f\varphi' + \frac{Nt}{Nb}\theta'' = 0 \tag{19}$$

The relative boundaries are

$$f = S, f' = 1 + s_f f'', \theta = 1 + s_\theta \theta', Ni\theta' + Nb\varphi' = 0 \text{ at } \eta = 0 \tag{20}$$

$$f' \rightarrow 0, \varphi \rightarrow 0, \theta \rightarrow 0, \text{ as } \eta \rightarrow \infty \tag{21}$$

The Sherwood number is

$$Sh = \frac{xq_m}{D_B(C_w - C_\infty)} \tag{22}$$

Here $q_m = -D_B\left(\frac{\partial C}{\partial y}\right)_{y=0}$

The Nusselt number is

$$Nu_x = \frac{xq_w}{k(T_w - T_\infty)} \tag{23}$$

Here $q_w = -k\left(\frac{\partial T}{\partial y}\right)_{y=0}$ and skin friction coefficient

$$C_f = \frac{2\tau_w}{\rho U_w^2} \tag{24}$$

Here $\tau_w = \mu\left(\frac{\partial u}{\partial y}\right)_{y=0}$

The final reduced forms of C_f and Nu are

$$C_f \text{Re}^{\frac{1}{2}} = 2\left(1 + \frac{1}{B}\right)f''(0) \tag{25}$$

$$(\text{Re}_x)^{-\frac{1}{2}}Nu_x = -\theta'(0) \tag{26}$$

$$(\text{Re}_x)^{-\frac{1}{2}}Sh = -\varphi'(0) \tag{27}$$

Here $\text{Re}_x = \frac{xU_w}{\nu}$

It is frequently feasible to identify base functions that are suitable to describe the solution, even without solving the given nonlinear issue, by studying the physical context and the initial/boundary conditions of the nonlinear differential equation.

3. Numerical solution

Transformed differential equations 17–19 with appropriate boundary conditions (20) and (21) are very nonlinear and have no analytical solution. They must be solved numerically using Matlab’s Runge-Kutta method with shooting technique. Higher-order differential equations become eight first-order simultaneous equations. In shooting approach, boundary value problems are converted to starting value problems. This technique converts the boundary value issue to initial conditions by treating boundary conditions as a function of starting circumstances at particular sites. From Table 1, it can be seen that present solver and previous results [40] and we conclude that an excellent agreement registered between the present solver and the previous reported work [40]. Fig. 2 describes the solution to the numerical procedure.

These are the primary phases of this numerical technique:

Table 1
Comparison of values of Nu for various Pr values when $B \rightarrow \infty, k_3 \rightarrow \infty, S = Sf = St = \beta = \lambda = A = 0$.

Pr	Ishak [39]	Present results
1	-0.9548	-0.954827
2	-1.4715	-1.471472
3	-1.8691	-1.869011
5	-2.5001	-2.500138
10	-3.6604	-3.660301

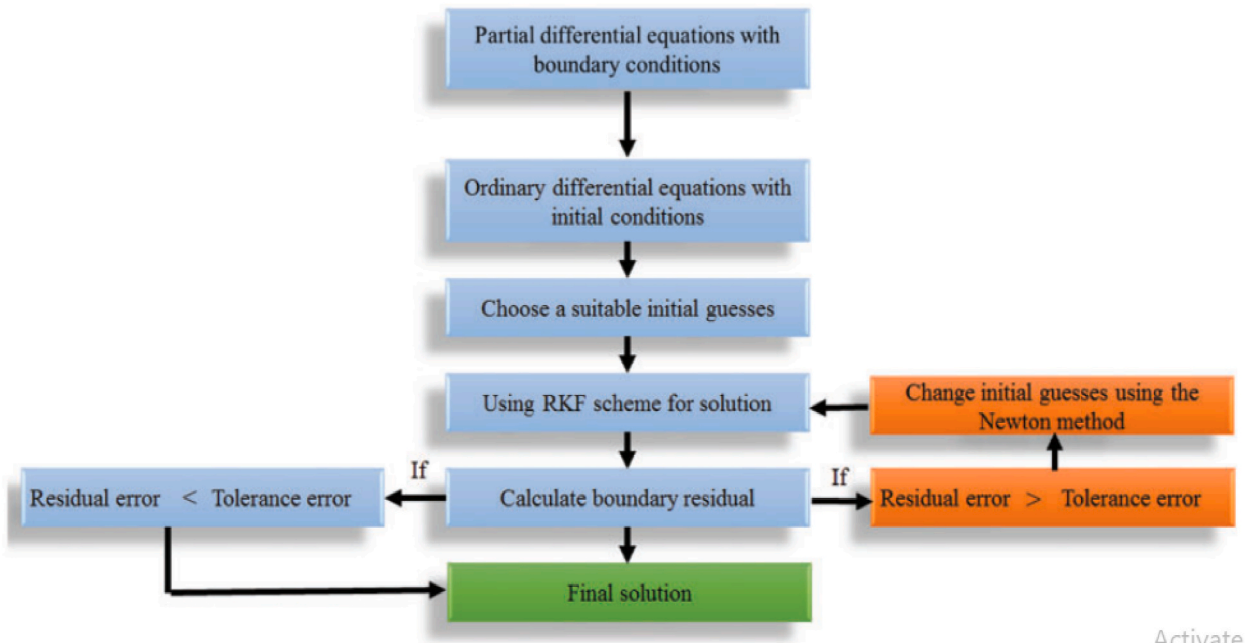


Fig. 2. Flow chart of the numerical solution.

Activate

1. Convert the boundary value issue to an initial value problem Eq. (28)

$$\left. \begin{aligned}
 f &= y(1, 1) \\
 f' &= y(2, 1) = dy(1, 1) \\
 f'' &= y(3, 1) = dy(2, 1) \\
 f''' &= dy(3, 1) \\
 \theta &= y(4, 1) \\
 \theta' &= y(5, 1) = dy(4, 1) \\
 \theta'' &= dy(5, 1) \\
 \varphi &= y(6, 1) \\
 \varphi' &= y(7, 1) = dy(6, 1) \\
 \varphi'' &= dy(7, 1)
 \end{aligned} \right\} \tag{28}$$

2. The flow equations along with boundary conditions transformed in to the following equations (29) and (30)

$$f''' = \frac{1}{\left(1 + \frac{1}{B}\right)} \left[-y(1, 1)y(3, 1) + y(2, 1)y(2, 1) + M^2y(2, 1) + \frac{y(2, 1)}{k_3} + \dots \right] \tag{29}$$

$$\theta'' = \frac{\text{Pr}}{\left(1 + Nr\right)} \left[A \left(y(4, 1) + \frac{\eta}{2}y(5, 1) \right) + \frac{2\beta[\epsilon + y(4, 1)]}{\text{Pr}(\eta + \alpha)^4} + \dots \right] \tag{30}$$

$$\varphi'' = -Ley(1, 1)y(7, 1) - \left(\frac{Nt}{Nb}\right) dy(5, 1) \tag{31}$$

3. The relative boundary conditions are used (32)

$$\left. \begin{aligned}
 & [y_a(1) - S \\
 & y_a(2) - 1 - S_f y_a(3) \\
 & y_a(4) - 1 - S_t y_a(5) \\
 & N_b y_a(7) + N_t y_a(4) \\
 & y_b(2) \\
 & y_b(4) \\
 & y_b(7)]
 \end{aligned} \right\} \tag{32}$$

First estimate beginning conditions of $y_3(0), y_5(0), y_7(0)$ without initial values. Eqs. 17–19 are integrated using R-K approach with 0.01 step iterations. First-order nonlinear coupled differential equations were solved using `bvp4c`. Check the supposed values by comparing the computed values $y_3(0), y_5(0), y_7(0)$ at $\eta = \eta_{max}$ and provided values at $\eta = \eta_{max}$. If their values vary, the operation is repeated until they match. We also use the Runge-Kutta technique to initialize with $y_3(0), y_5(0), y_7(0)$ and integrate Eqs. 28–32. This method is continued until the planned value and provided condition settle within precision 10^{-5} .

4. Results and discussion

A descriptive numerical analysis of various constraints are explained here. To varying one governing factor, we fixed the remaining parameters as constant. Blood flow velocity, blood flow temperature, Concentration, Cf, Nu and Sh have been examined in details with the effects of Solutal, thermal and fluid flow governing parameters. We assumed the following values to get plots. $S = 1, Pr = 23, A = 1, \epsilon = 78.5, Nr = 1, sf = 2.5, st = 1.5, k_3 = 0.3, \alpha = \beta = M = 1, Le = 0.5, Nt = Nb = 0.1$.

Fig. 3 depicts an impact of Casson parameter on blood flow velocity. From this figure, we have the boundary layer depreciates as the Casson parameter values improvements. Fig. 3 shows an impact of ferromagnetic parameter on blood flow velocity created by a magnetic dipole. When noted in Fig. 4, the blood flow velocity falls as the magnetic region operates to enhance the retarding force, but the blood flow temperature profile exhibits the opposite tendency (Fig. 14). Figs. 5 and 15 depicts an impact of magnetic parameter on blood flow velocity and blood flow temperature. Noted that fluid blood flow velocity declined as the magnetic field factor increased, and the boundary layer blood flow temperature heightened as well. This demonstrates exactly how transport processes are opposed by magnetic field. As the magnetic field parameter increased, we can observe that the fluid blood flow velocity decreased and the boundary layer blood flow temperature heightened in the same situation. As a result, the transverse magnetic field has a propensity to produce the Lorentz force, a drag force [41,42]. A change in the surface area to liquid interface causes a rise in the heat transfer rate. Similarly, the increased liquid blood flow temperature may be detected. Fig. 6 shows an impact of permeability parameter on blood flow velocity. Fig. 6 illustrates how the blood flow velocity profile improves as the permeability parameter rises (k_3). The blood flow velocity and blood flow temperature profiles for distinct values of the porous permeability parameter K_3 are shown in Figs. 6 and 16, respectively. Physically, porous medium reduces the resistance to the flow, the fluid blood flow velocity increases as the value of the porosity parameter K_3 rises, but the blood flow temperature profile follows the opposite pattern. Fig. 7 shows an impact of Prandtl number on blood flow velocity. Physically, there is a direct correlation between the Prandtl number and momentum diffusivity, changes in the Prandtl number may be used to track the behaviour of velocities as they increase. Momentum diffusivity grows in tandem with the Prandtl parameter, leading to a corresponding expansion of fluid motion and boundary layer thickness. Fig. 8 displays suction parameter impact on blood flow velocity. Fig. 8 shown the blood flow velocity decreases as the suction parameter improvements. Physically, the thickening of the momentum boundary layer decreases in blood flow velocity are both obvious from the

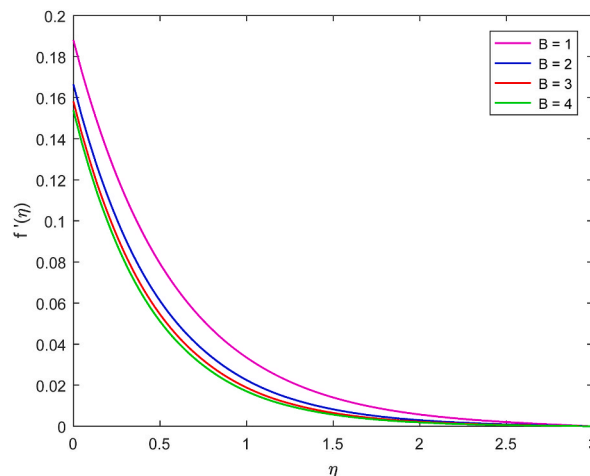


Fig. 3. Plot of f' field for various values B.

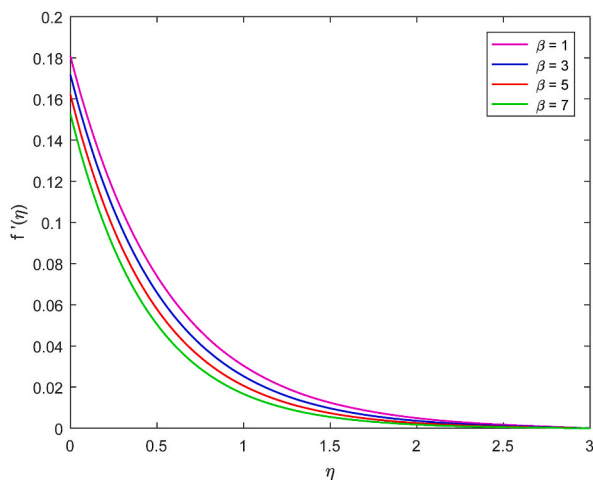


Fig. 4. Plot of f' field for various values β .

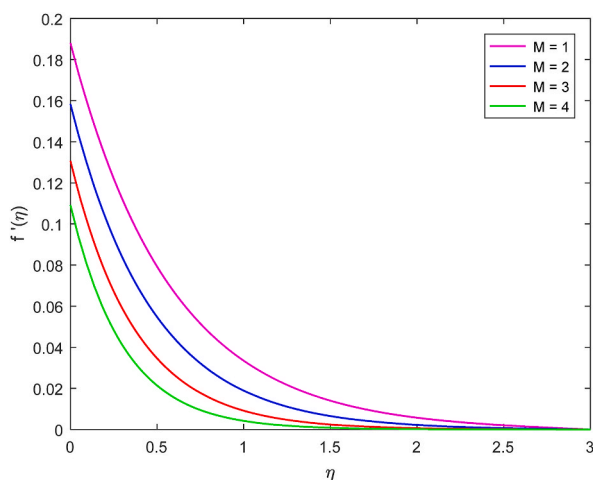


Fig. 5. Plot of f' field for various values M .

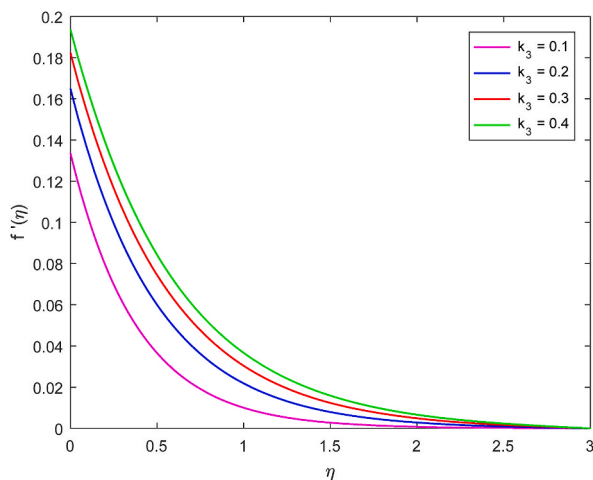


Fig. 6. Plot of f' field for various values k_3 .

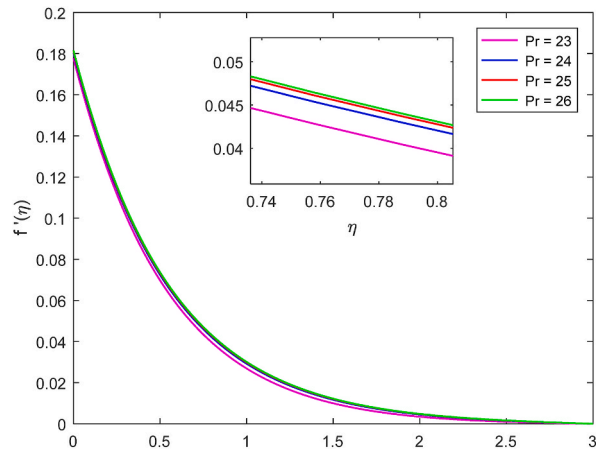


Fig. 7. Plot of f' field for various values Pr.

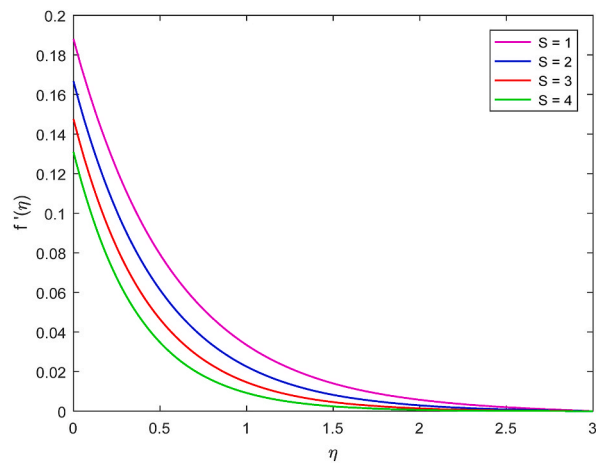


Fig. 8. Plot of f' field for various values S.

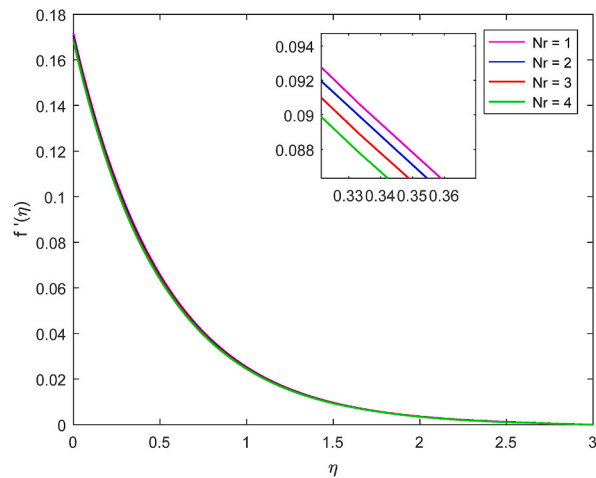


Fig. 9. Plot of f' field for various values Nr.

diagram, indicating that these values for S are rather conservative. Figs. 9 and 19 show that fluid blood flow velocity decreases with increasing radiation parameter values, whereas blood flow temperature profile in this instance improvements. Blood flow temperature profiles advance because the fluid’s conduction effects in the presence of radiation do. Fig. 10 demonstrates how the blood flow velocity profile improves as the thermal slip factor does. Fig. 19 shows thermal radiation parameter Nr impact on blood flow velocity profile. In Fig. 11, the fluid blood flow velocity profile is shown to deteriorate as the blood flow velocity slip factor improvements. Clearly, the blood flow velocity reduces monotonically to zero as one moves away from the solid surface when slip is present at the fluid-solid interface. If the fluid blood flow velocity next to the solid surface is equal to the blood flow velocity of the stretched sheet, as shown in Fig. 11, then $f'(0) = 1$, indicating that the no-slip condition holds. It happens because, under slip circumstances, a portion of the sheet’s drag is transferred to the fluid. As the values of the unsteadiness parameter (A) progress, it can be seen in Fig. 12 that the boundary layer improves. The results are qualitatively correct in the chosen values of unsteady parameter. Momentum boundary layer decays with unsteadiness parameter A .

Fig. 13 demonstrates how, at a certain time, it is discovered that the blood flow temperature improvements. Physically, the Casson parameter assists to the strengthened blood flow temperature gradients in the boundary layer. Fig. 14 illustrates how the blood flow temperature profile improves in this situation. Noted that the ferromagnetic number and kelvin force, also known as drug force. Fig. 16 demonstrates how the blood flow temperature distribution declines as the permeability parameter’s values rise (k_3). Physically, blood flow temperature declines for higher values of k_3 near the boundary layer. Fig. 17 shows that the blood flow temperature declines with increasing Prandtl number values as a result of the advancement of fluid heat capacity or the decline of thermal diffusivity. Physically, the improvement of Prandtl number means slow rate of thermal diffusion. As the suction parameter (S) value improvements, the blood flow temperature profile in the flow zone decreases, as shown in Fig. 18. Thermal boundary layer thickness decreases as the suction parameter improvements because more fluid is removed from the fluid region. Physically, both the blood flow temperature and the thickness of the thermal boundary layer are reduced, representing significant under-estimates of S . According to Fig. 20, blood flow

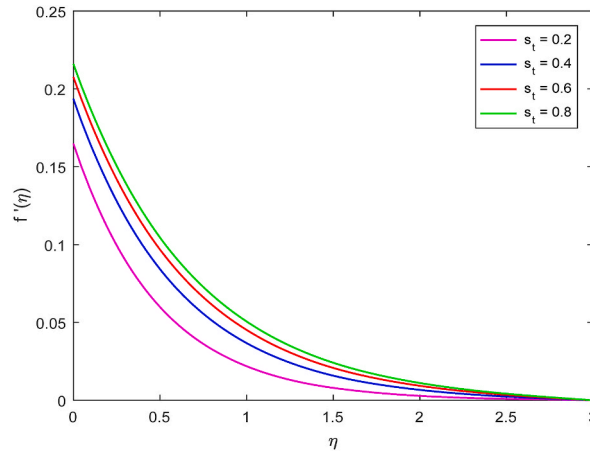


Fig. 10. Plot of f' field for various values St .

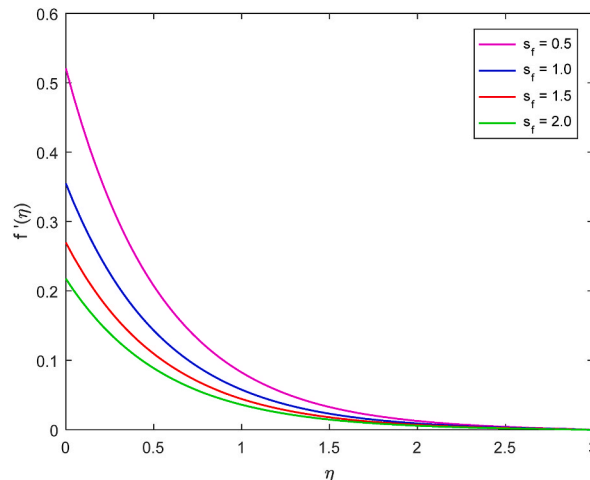


Fig. 11. Plot of f' field for various values Sf .

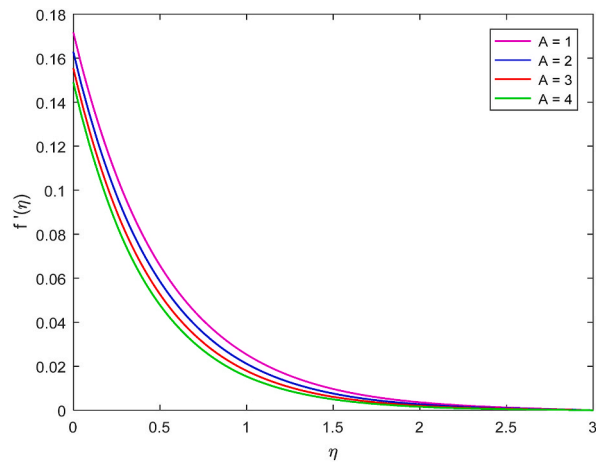


Fig. 12. Plot of f' field for various values A.

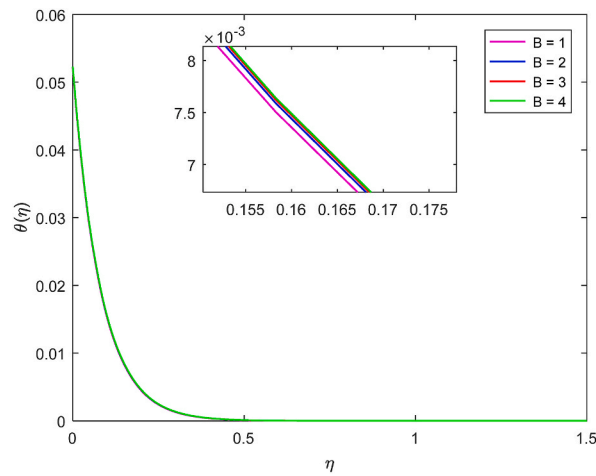


Fig. 13. Plot of θ field for various values B.

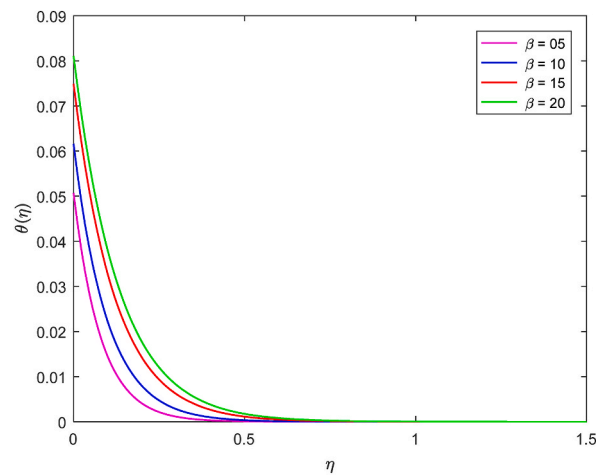


Fig. 14. Plot of θ field for various values β .

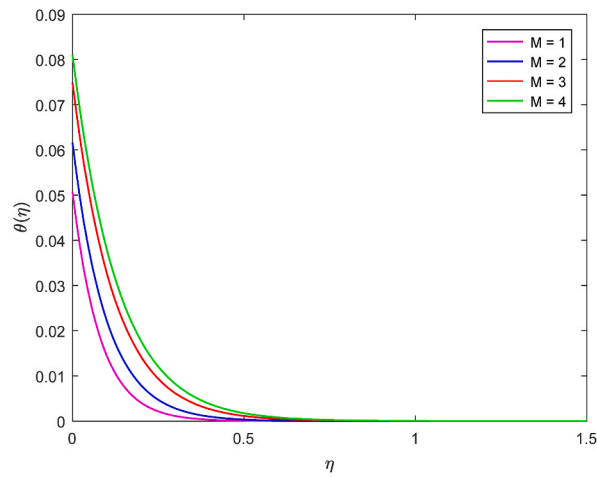


Fig. 15. Plot of θ field for various values M .

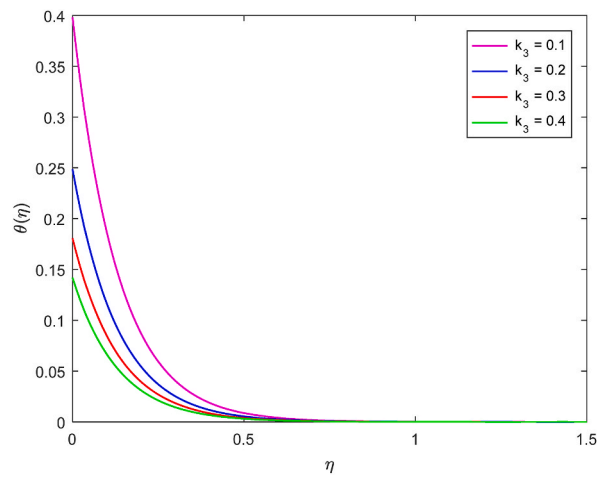


Fig. 16. Plot of θ field for various values k_3 .

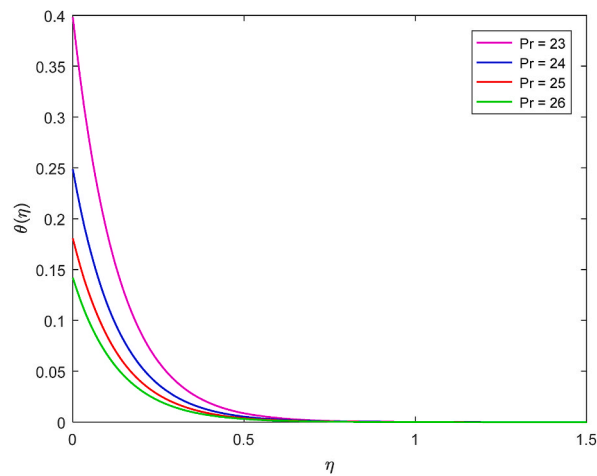


Fig. 17. Plot of θ field for various values Pr .

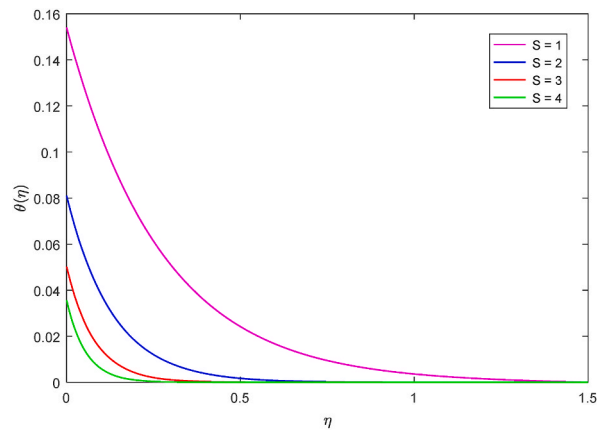


Fig. 18. Plot of θ field for various values S .

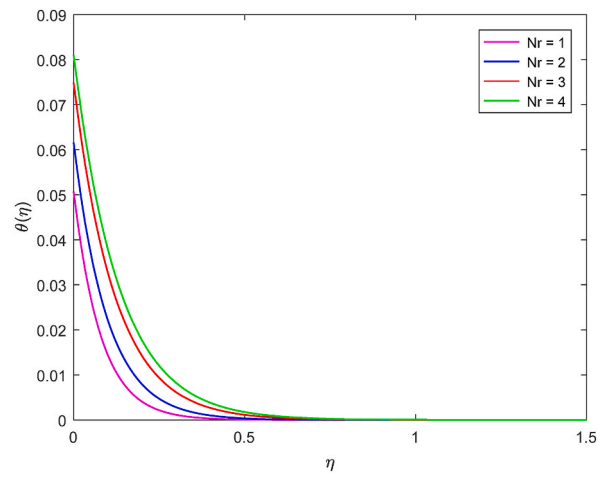


Fig. 19. Plot of θ field for various values Nr .

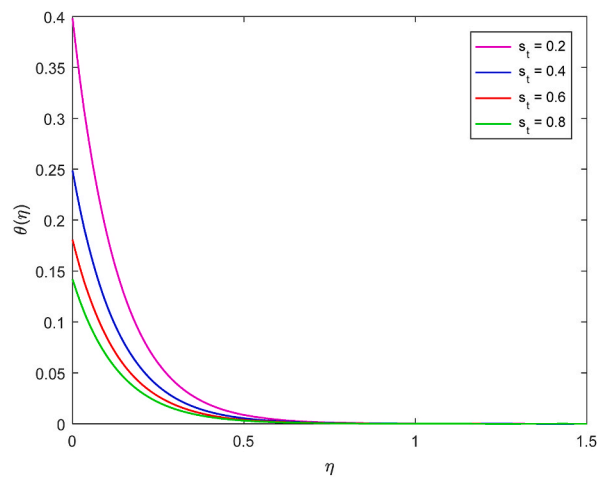


Fig. 20. Plot of θ field for various values St .

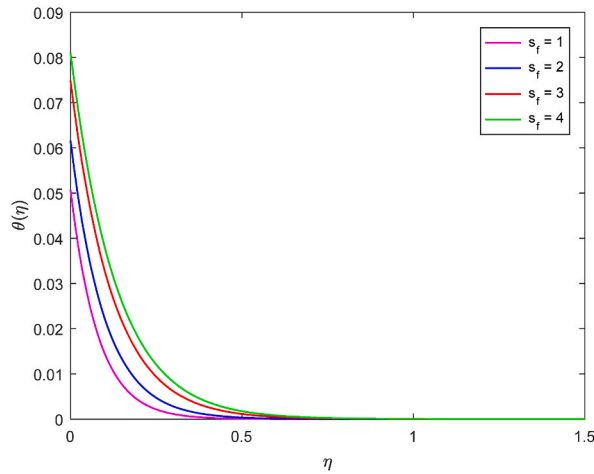


Fig. 21. Plot of θ field for various values Sf.

temperature decreases as the thermal slip factor (St) improvements. Due to the thermal slip factor, heat is transferred from the stretched sheet to the fluid. According to Fig. 21, the blood flow temperature profile improves with improving values of the blood flow velocity slip factor at every position in the flow sheet. Physically, an enhance in the blood flow velocity slip parameter inclines and increases the blood flow fluid temperature and reduce the blood flow temperature gradient, which epitomizes heat transfer rate. Fig. 22 demonstrates how the blood flow temperature is discovered to decline with advancement at a certain stage. As a result of the slow loss of heat transmitted from the region to the liquid, and noted that, transferred heat from the sheet to the fluid depreciates as the parameter of unsteadiness improvements. Thermal boundary layer decays with unsteadiness parameter A.

Fig. 23 displays the effect of thermophoresis parameter, Nt, on the concentration distributions. Thermophoresis is the movement of particles owing to the blood flow temperature gradient force. Nt affects nanoparticle volume fraction. Increasing Nt improves the concentration profile. As Nt grows, heat transmission in the boundary layer rises and particle deposition away from the fluid area worsens, increasing nanoparticle volume fraction. Fig. 24 shows how Nb affects concentration distributions. Nb vales reduce nanoparticle concentration. Because of spontaneous diffusivity, nanoparticles rearrange. The nanofluid’s thermal conductivity improves. Brownian motion heats the boundary layer fluid and rages particles away from the fluid system, lowering concentration distributions. Fig. 25 shows how Le affects concentration distributions. Increasing Le decreases concentration profiles and boundary layer thickness. Le indicates momentum-to-mass diffusion. Mass diffusivity reduces concentration.

From Table 2, we observe that Skin-friction coefficient progress with heightening values of Nr, A, β , B and M where as declines with heightening values of S, k_3 and α . From Table 3, we observe that Nusselt number progress with heightening values of Pr, S and k_3 where as decreases Nr, A, b and M. From Table 4, we observe that the Sherwood number progress with heightening values of Nt while decreases with Nb.

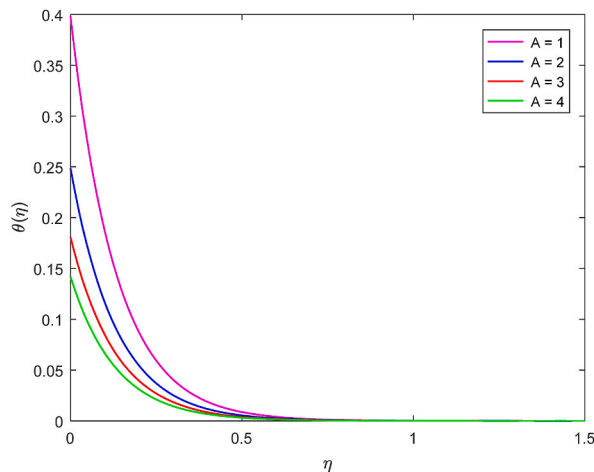


Fig. 22. Plot of θ field for various values A.

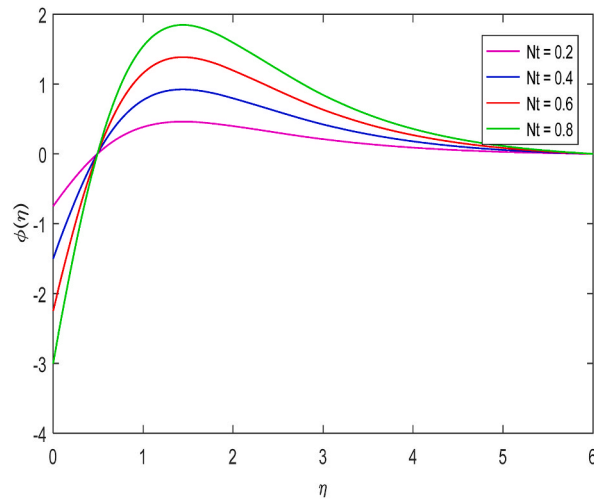


Fig. 23. Plot of ϕ field for various values Nt .

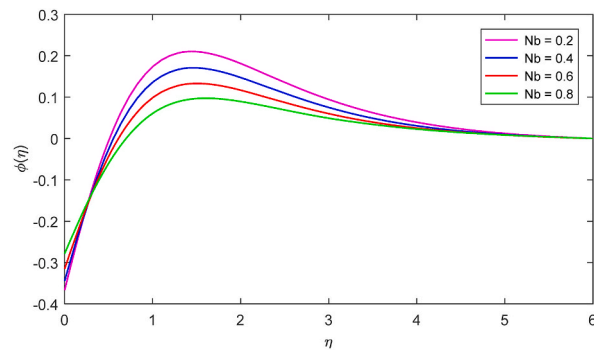


Fig. 24. Plot of ϕ field for various values Nb .

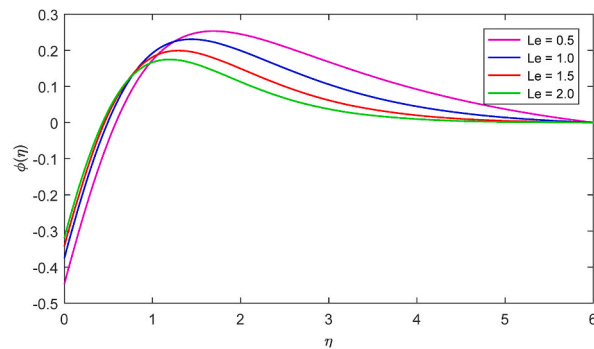


Fig. 25. Plot of ϕ field for various values Le .

5. Conclusions

The applications of magnetic dipole ferromagnetic non-Newtonian radiative MHD blood flow have been worked out. The slip effects phenomenon has been utilized. RK-4 approach quantitatively solves the issue. Mat lab is used for graphical analysis. Below are the primary flow points:

- The heightening value of ferromagnetic interaction in the blood flow temperature field is improved and the blood flow velocity domain is declined when magnetic dipole is applied.

Table 2
Skin-friction for various parameter values.

Nr	A	S	k_3	α	β	B	M	Cf
1								0.3271
2								0.3272
3								0.3273
4								0.3274
	0.1							0.3264
	0.2							0.3265
	0.3							0.3266
	0.4							0.3267
		1						0.3271
		2						0.3354
		3						0.3427
		4						0.3491
			0.1					0.3466
			0.2					0.3340
			0.3					0.3271
			0.4					0.3225
				0.1				0.3280
				0.2				0.3277
				0.3				0.3275
				0.4				0.3274
					1			0.3271
					2			0.3272
					3			0.3273
					4			0.3274
						1		0.3271
						2		0.3358
						3		0.3392
						4		0.3405
							0.5	0.3230
							1	0.3271
							1.5	0.3325
							2	0.3383

Table 3
Nusselt number for various parameter values.

Nr	Pr	A	S	k_3	B	M	Nu
1							1.2267
2							1.1907
3							1.1604
4							1.1341
	21						1.2193
	22						1.2231
	23						1.2267
	24						1.2300
		0.1					1.2593
		0.2					1.2564
		0.3					1.2533
		0.4					1.2501
			1				1.2267
			2				1.2859
			3				1.3036
			4				1.3118
				0.1			1.2253
				0.2			1.2262
				0.3			1.2267
				0.4			1.2270
					1		1.2267
					2		0.9195
					3		0.8172
					4		0.7661
						0.5	1.2269
						1	1.2267
						1.5	1.2263
						2	1.2259

Table 4
Sherwood number for various parameter values.

Nt	Nb	Sh
0.2		1.2267
0.4		2.4533
0.6		3.6800
0.8		4.9067
	0.2	0.3067
	0.4	0.1533
	0.6	0.1022
	0.8	0.0767

- Blood flow velocity is reduces with heightening Magnetic parameter value whereas opposite trend is noted for blood flow temperature.
- Casson parameter causes a noticeable shift in blood flow velocity magnitude. Due to the interplay of the momentum slip phenomena, the blood flow velocity was regulated.
- As the permeability parameter increases, the observed rate of blood flow velocity variation also increases.
- Momentum and thermal boundary layers decays with unsteadiness parameter A.
- Thermal radiation parameter enhances the blood flow temperature field.
- Blood flow temperature decreases for higher values of Pr.
- Blood flow temperature decreases for higher values of k_3 near the boundary layer.
- The blood flow temperature accelerates for distinct values of Cassson parameter, but it shows opposite behaviour for escalated integrity of suction parameter.
- Skin friction coefficient heightens with the variation of ferromagnetic interaction parameter and Hartmann number.
- Nusselt number is reduces with the variation of thermal radiation parameter.
- Casson parameter increases skin-friction and reduces Nusselt number.

Author contribution statement

G. Dharmaiah: Conceived and designed the experiments; Analyzed and interpreted the data; Wrote the paper.

J. L. Rama Prasad: Performed the experiments; Analyzed and interpreted the data; Wrote the paper.

K. S. Balamurugan: Performed the experiments; Analyzed and interpreted the data; Contributed reagents, materials, analysis tools or data; Wrote the paper.

I. Nurhidayat: Performed the experiments; Analyzed and interpreted the data; Contributed reagents, materials, analysis tools or data.

Unai Fernandez-Gamiz: Conceived and designed the experiments; Contributed reagents, materials, analysis tools or data.

Samad Noeiaghdam: Conceived and designed the experiments; Contributed reagents, materials, analysis tools or data; Wrote the paper.

Funding statement

Unai Fernandez-Gamiz was supported by Government of the Basque Country [ELKARTEK21/10KK-2021/00014 & ELKARTEK22/85].

Irfan Nurhidayat was supported by King Mongkut's Institute of Technology Ladkrabang (KMITL), Bangkok, Thailand [KDS2020/045].

Data availability statement

No data was used for the research described in the article.

Declaration of interest's statement

The authors declare no conflict of interest.

Abbreviation

C_p	specific heat at constant pressure(J/kg.K)
H	magnetic field of density(A/m)
M_1	magnetization(A/m)
T_∞	fluid blood flow temperature far away from the sheet(K)
T_w	blood flow temperature of the sheet(K)

T	fluid blood flow temperature inside the boundary layer(K)
t	time(s)
x, y	horizontal and vertical coordinates(m)
u, v	horizontal and vertical velocities(m/s)
B	Casson parameter
a,b,c	constants
N	blood flow velocity slip factor
K	thermal slip factor
U _w	stretching blood flow velocity
V _w	suction/injection blood flow velocity
C _f	skin-friction coefficient
q _r	radiative heat flux
B(t)	time-dependent magnetic field intensity
k ₂	constant permeability medium
k*	mean absorption coefficient
A	unsteady parameter
Nu	local nusselt number
q _w	wall heat flux
Re	local Reynolds number
k ₁ (t)	time-dependent magnetic permeability
k ₃	non-dimensional permeability parameter
d	distance between magnetic dipole to the sheet

Greek Symbols

κ	thermal conductivity(J/msK)
σ	electrical conductivity of the fluid(S/m)
μ_0	magnetic permeability(kg.m/A ² s ²)
ν	kinetic viscosity(m ² /s)
μ	dynamic viscosity(kg/ms)
ρ	density of the fluid(kg/m ³)
η	similarity variable
β	ferromagnetic interaction parameter
θ	dimensionless blood flow temperature

References

- [1] Md. Ghulam Murtaza, Efstratios Emmanouil Tzirtzilakis, Mohammad Ferdows, Stability and convergence analysis of a biomagnetic fluid flow over a stretching sheet in the presence of a magnetic field, 2020, *Symmetry* 12 (2020) 253, <https://doi.org/10.3390/sym12020253>.
- [2] M.G. Murtaza, E.E. Tzirtzilakis, M. Ferdows, Effect of electrical conductivity and magnetization on the biomagnetic fluid flow over a stretching sheet, *Z. Angew. Math. Phys.* 68 (2017) 93.
- [3] A. Ogulu, E. Amos, Modeling Pulsatile blood flow within a homogeneous porous bed in the presence of a uniform magnetic field and time dependent suction, *Int. Commun. Heat Mass Tran.* 34 (2007) 989–995.
- [4] S.N. Majhi, V.R. Nair, Pulsatile flow of third grade fluids under body acceleration modeling blood flow, *Int. J. Eng. Sci.* 32 (1994) 839–846.
- [5] A. Zaman, N. Ali, M. Sajid, Numerical Simulation of Pulsatile flow of blood in a porous saturated overlapping stenosed artery, *Math. Comput. Simulat.* 134 (2017) 1–16.
- [6] J. Alam, G. Murtaza, E. Tzirtzilakis, M. Ferdows, Biomagnetic fluid flow and heat transfer study of blood with gold nanoparticles over a stretching sheet in the presence of magnetic dipole, *Fluid* 6 (2021) 113, <https://doi.org/10.3390/fluids6030113>.
- [7] K.K. Olubode, L.C. Issac, B. Mahanthesh, S. Salman, Heat transfer in the flow of Blood-gold carreau nanofluid induced by partial slip and buoyancy, *Heat Tran. Asian Res.* 47 (2018) 806–823.
- [8] M.J. Alam, M.G. Murtaza, Two Dimensional Biomagnetic fluid flow and heat transfer over a nonlinear stretching sheet with temperature dependent viscosity, *Sch. J. Phys. Math. Stat.* 7 (2020) 131–142.
- [9] M.G. Murtaza, M. Ferdows, J.C. Misra, E.E. Tzirtzilakis, Three-dimensional biomagnetic Maxwell fluid flow over a stretching surface in presence of heat source/sink, *Int. J. Biomath.* 12 (2019), 1950036-20.
- [10] H. Jung, J. Choi, C. Park, Asymmetric flows of non-newtonian fluids in a symmetric stenosed artery, *Korea Aust. Rheol. J.* 1 (2004) 101–108.
- [11] T. Sochi, Non-Newtonian Rheology in Blood Circulation, in: *Fluid Dynamics*, vol. 1, Department of Physics and Astronomy, University College London, London, UK, 2014.
- [12] Muhammad Khairul Anuar Mohamed, Siti Hanani Mat Yasin, Mohd Zuki Salleh, Hamzeh Taha Alkasasbeh, MHD stagnation point flow and heat transfer over a stretching sheet in a blood-based casson Ferro fluid with Newtonian heating, 2021, *J. Adv. Res. Fluid Mech. Therm. Sci.* 82 (1) (2021) 1–11.
- [13] Nattawan Chuchalerm, Wannika Sawangtong, Benchawan Wiwatanapataphee, Thanongchai Siriapisith, Study of non-Newtonian blood flow - heat transfer characteristics in the human coronary system with an external magnetic field, *Math. Biosci. Eng.* 19 (9) (2022) 9550–9570.
- [14] K. Bhupendra, Sharma and Chandan Kumawat, Impact of temperature dependent viscosity and thermal conductivity on MHD blood flow through a stretching surface with ohmic eect and chemical reaction, *Nonlinear Eng.* 10 (2021) 255–271.
- [15] Cedric Gervais Njingang Ketchate, Pascaline Tiam Kapen, Didier Fokwa, Ghislain Tchuen, Stability analysis of non-Newtonian blood flow conveying hybrid magnetic nanoparticles as target drug delivery in presence of inclined magnetic field and thermal radiation: application to therapy of cancer, *Inform. Med. Unlocked* 27 (2021), 100800, <https://doi.org/10.1016/j.imu.2021.100800>.

- [16] T. Hamzeh, Alkassasbeh, numerical solution of heat transfer flow of casson hybrid nanofluid over vertical stretching sheet with magnetic field effect, *CFD Lett.* 14 (3) (2022) 39–52.
- [17] E. Akinbobola Temitope, Samuel S. Okoya, The flow of second grade fluid over a stretching sheet with variable thermal conductivity and viscosity in the presence of heat source/sink, *J. Niger. Math. Soc.* 34 (3) (2015) 331–342.
- [18] Ghulam Rasool, Ali J. Chamkha, Taseer Muhammad, Anum Shafiq, Ilyas Khan, Darcy-Forchheimer relation in Casson type MHD nanofluid flow over non-linear stretching surface, *Propuls. Power Res.* 9 (2) (2020) 159–168.
- [19] Abdelmalek Zahra, B. Mahanthesh, Md Basir Md Faisal, Imtiaz Maria, Mackolil Joby, Khan Noor Saeed, A. Nabwey Hossam, I. Tlili, Mixed radiated magneto Casson fluid flow with Arrhenius activation energy and Newtonian heating effects: flow and sensitivity analysis, *Alex. Eng. J.* 59 (2020) 3991–4011.
- [20] Charan Kumar Gandeta, Dharmiaiah Gurram, K.S. Balamurugan, Vedavathi Nallapati, Chemical reaction AndSoret effects on casson Mhd fluid over A vertical plate, *Int. J. Chem. Sci.* 14 (1) (2016) 213–221. ISSN 0972-768X.
- [21] Vedavathi Nallapati, Dharmiaiah Gurram, K.S. Balamurugan, Charan Kumar Gandeta chemical reaction, radiation and Dufour effects on casson magneto hydro dynamics fluid flow over A vertical plate with heat source/sink, *Global J. Pure Appl. Math.* XII (1) (2016) 191–200. ISSN 0973-1768.
- [22] T. Hayat, S. Ahmad, M.I. Khan, A. Alsaedi, Simulation of ferromagnetic nanomaterial flow of Maxwell fluid, *Results Phys.* 8 (2018) 34–40.
- [23] L. Ali, X. Liu, B. Ali, S. Mujeed, S. Abdal, S.A. Khan, Analysis of magnetic properties of nano-particles due to a magnetic dipole in micropolar fluid flow over a stretching sheet, *Coatings* 10 (2020) 170.
- [24] G. Rasool, A. Shafiq, M.S. Alqarni, A. Wakif, I. Khan, M.S. Bhutta, Numerical scrutinization of Darcy-forchheimer relation in convective magnetohydrodynamic nanofluid flow bounded by nonlinear stretching surface in the perspective of heat and mass transfer, *Micromachines* 12 (4) (2021) 374.
- [25] B. Saleh, J.K. Madhukesh, R.S. Varun Kumar, A. Afzal, Y. Abdelrhman, A.A. Aly, R.J. Punith Gowda, Aspects of magnetic dipole and heat source/sink on the Maxwell hybrid nanofluid flow over a stretching sheet, *Proc. IME E J. Process Mech. Eng.* (2022), <https://doi.org/10.1177/09544089211056243>.
- [26] Y. Veeranna, M.C. Jayaprakash, G.T. Sreenivasa, K.R. Lalitha, Effect of stefan blowing and magnetic dipole on chemically reactive second-grade nanomaterial flow over stretching sheet, *Int. J. Ambient Energy* 12 (2021) 1–25, <https://doi.org/10.1080/01430750.2021.1999325>.
- [27] Y. Kobu, Effects of infrared radiation on intraosseous blood flow and oxygen tension in rat tibia, *Kobe J. Med. Sci.* 45 (1999) 27–39.
- [28] S. Inoue, M. Kobaya, Biological activities caused by far infrared radiation, *Int. J. Biometeorol.* 33 (1989) 145–150.
- [29] C. Nishimoto, Y. Ishiura, K. Kuniyasu, T. Koga, Effects of ultrasonic radiation on cutaneous blood flow in the paw of decerebrated rats, *Kawasaki J. Med Welfare* 12 (2006) 13–18.
- [30] A. Ogulu, A.R. Bestman, Blood flow in a curved pipe with radiative heat transfer, *Acta Phys. Hung.* 74 (1994) 189–201.
- [31] I.H. Chen, Analysis of an intensive magnetic field on blood flow: part 2, *J. Bioelectr.* 4 (1985) 55–61.
- [32] E.E. Tzirtzilakis, G.B. Tanoudis, Numerical study of biomagnetic fluid flow over a stretching sheet with heat transfer, *Int. J. Numer. Methods Heat Fluid Flow* 13 (2003) 830–848.
- [33] S. Srinivas, P.B.A. Reddy, B.S.R.V. Prasad, Effects of magnetic reaction and thermal radiation on Mhd flow over an inclined permeable stretching surface with NonUniform heat source/sink: an application to the dynamics of blood flow, *J. Mech. Med. Biol.* 14 (5) (2014), 1450067, <https://doi.org/10.1142/S0219519414500675>.
- [34] J.C. Misra, A. Sinha, Effect of thermal radiation on MHD flow of blood and heat transfer in a permeable capillary in stretching motion, *Heat Mass Tran.* 49 (2013) 617–628, <https://doi.org/10.1007/s00231-012-1107-6>.
- [35] L. Wahidunnsia, K. Subbarayudu, S. Suneetha, A novel technique for unsteady Newtonian fluid flow over a permeable plate with viscous dissipation, non-uniform heat source/sink and chemical reaction, *Int. J. Res. Eng. Appl. Manag.* 4 (10) (2019) 58–67.
- [36] N. Vedavathi, G. Dharmiaiah, S. Noeiaghdam, U. Fernandez-Gamiz, A chemical engineering application on hyperbolic tangent flow examination about sphere with Brownian motion and thermophoresis effects using BVP5C, *Case Stud. Therm. Eng.* (2022), 102491.
- [37] G. Dharmiaiah, W. Sridhar, Khaled AL-Farhany, K. S. Balamurugan, Farhan Ali, Non-Newtonian nanofluid characteristics over a melting wedge: a numerical study, *Heat Transfer*, Accepted: 11 March 2022.
- [38] Gurram Dharmiaiah, Saeed Dinarvand, K. S. Balamurugan, MHD radiative ohmic heating nanofluid flow of a stretching penetrable wedge: a numerical analysis, *Heat Transfer*, Accepted: 6 March 2022.
- [39] M. Senapati, S.K. Parida, K. Swain, S.M. Ibrahim, Analysis of variable magnetic field on chemically dissipative MHD boundary layer flow of Casson fluid over a nonlinearly stretching sheet with slip conditions, *Int. J. Ambient Energy* (2020) 1–15.
- [40] A. Ishak, MHD boundary layer flow due to an exponentially stretching sheet with radiation effect, *Sains Malays.* 40 (4) (2011) 391–395.
- [41] N. Hameed, S. Noeiaghdam, W. Khan, B. Pimpunchat, U. Fernandez-Gamiz, M. Sohail Khan, A. Rehman, Analytical analysis of the magnetic field, heat generation and absorption, viscous dissipation on couple stress Casson hybrid Nano fluid over a nonlinear stretching surface, *Results Eng.* 16 (2022), 100601, <https://doi.org/10.1016/j.rineng.2022.100601>.
- [42] P. Thyagarajan, S. Sathiamoorthy, H. Balasundaram, O.D. Makinde, U. Fernandez-Gamiz, S. Noeiaghdam, S.S. Santra, M. Altanji, Mass transfer effects on mucus fluid in the presence of chemical reaction, *Alex. Eng. J.* 62 (2023) 193–210, <https://doi.org/10.1016/j.aej.2022.06.030>.